Article

Performance of an Adaptive Optimization Paradigm for Optimal Operation of a Mono-Switch Class E Induction Heating Application

Saddam Aziz [1,*], Cheung-Ming Lai [1] and Ka Hong Loo [1,2,*]

[1] Centre for Advances in Reliability and Safety, New Territories, Hong Kong, China; denny.lai@cairs.hk
[2] Department of Electronic and Information Engineering, The Hong Kong Polytechnic University (PolyU), Hong Kong, China
* Correspondence: saddam.aziz@cairs.hk (S.A.); kh.loo@polyu.edu.hk (K.H.L.)

Abstract: The progress of technology involves the continuous improvement of current machines to attain higher levels of energy efficiency, operational dependability, and effectiveness. Induction heating is a thermal process that involves the heating of materials that possess electrical conductivity, such as metals. This technique finds diverse applications, including induction welding and induction cooking pots. The optimization of the operating point of the inverter discussed in this study necessitated the resolution of a pair of non-convex mathematical models to enhance the energy efficiency of the inverters and mitigate switching losses. In order to determine the most advantageous operational location, a sophisticated surface optimization was conducted, requiring the implementation of a sophisticated optimization methodology, such as the adaptive black widow optimization algorithm. The methodology draws inspiration from the resourceful behavior of female black widow spiders in their quest for nourishment. Its straightforward control variable design and limited computational complexity make it a feasible option for addressing multi-dimensional engineering problems within confined constraints. The primary objective of utilizing the adaptive black widow optimization algorithm in the context of induction heating is to optimize the pertinent process parameters, including power level, frequency, coil design, and material properties, with the ultimate goal of efficiently achieving the desired heating outcomes. The utilization of the adaptive black widow optimization algorithm presents a versatile and robust methodology for addressing optimization problems in the field of induction heating. This is due to its capacity to effectively manage intricate, non-linear, and multi-faceted optimization predicaments. The adaptive black widow optimization algorithm has been modified in order to enhance the optimization process and guarantee the identification of the global optimum. The empirical findings derived from an authentic inverter setup were compared with the hypothetical results.

Keywords: artificial intelligence; induction cooker; optimal structure and energy reliability of cookware

MSC: 65K10; 68T05

1. Introduction

Due to its superior efficacy, efficient control [1,2], and minimal gaseous emissions, induction heating has been broadly adopted, not only in industrial applications, but also in household appliances [3,4]. Induction heating procedures (IHPs) have several characteristics that are superior to electric burners and gas cooking burners, including quicker warming rates, lower energy usage and expenses, no harmful greenhouse gases emissions, touchless scorching that is secure, and compact sizes [5]. The primary components of a household IHP system are the power circuit design, the process control, the coil, and the cooking utensils [6].

There is a wide variety of cookware available, each of which can have an impact on how well an IHP system functions due to differences in size and thickness. Furthermore, the diverse cooking behaviors have an impact on the monitoring process variables of the IHP system [7]. Additionally, heating and shifting cycles can alter the precision of the cookware load measurement made by the IHP system, thereby compromising the dependability of the voltage-controlled circuit and management equipment [8]. In all cases, more precise temperature control is required for compact manufacturing and the electricity-saving demands of today [9,10], increasing the importance of an optimal design [11,12].

Voltage-controlled modules with higher current densities require precision control, especially when interacting with devices operating at higher frequencies, such as IHP systems. The components of a mono-switch voltage-source quasi-resonant inverter are depicted in Figure 1 [13]. In this study, a class E inverter is used as the converter, as has been mentioned in the literature, especially in relation to its uses in induction cookers, which typically operate between 20 kHz and 50 kHz [14].
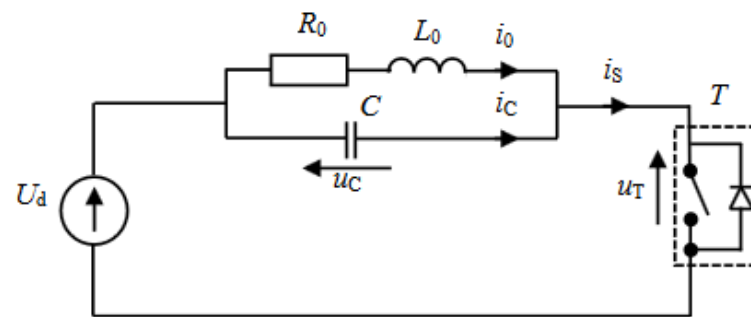

Figure 1. Simple mono-switch inverter circuit diagram.

For induction stoves and burners to produce the desired heating effects (such as surface heating), or to meet technological criteria, a significantly higher frequency is typically employed [15,16]. The converter switching frequency is bounded by its commutation capabilities, as was mentioned earlier. Therefore, particularly in high-frequency units, the problem of reducing conduction loss in the converter is of paramount importance [17]. The study in [18] examined the inverter represented in Figure 1, which operates at cycles of several hundred kilohertz. Optimization of the inverter's operating point and circuit analysis employing the time-tested Hook–Jeeves technique is outlined in [5]. Assuming perfect circumstances, multiple charges (ferrous and non-ferromagnetic shafts of varied sizes) were measured. The power density, as well as system losses, were investigated using measured results to assess the impact of charge and the system capacitor [19]. Low switching losses can be achieved by finding the best operating point for the inverter. The authors in [12] examined the systems' energy efficacy and the causes of losses. Capacitance within the system and its impact on electrical efficiency as a whole were also studied [20].

The solution to two non-convex models is required in order to determine the appropriate operating settings of the inverter. These equations generate a complicated topography search that includes a large number of local minima. Villa et al. [21] proposed a deep learning approach for induction heating applications, and the suggested approach was implemented in an experimental prototype equipped with a system-on-chip. Nevertheless, the strategy's viability is highly dependent on the selected data set. If the data had not been selected appropriately, the program would have produced erroneous predictions.

Meta-heuristics are a type of optimization strategy that consists of a set of sophisticated algorithms that apply heuristics in an intelligent manner to identify reasonably close solutions to intricate optimization problems [22] rapidly and effectively [23,24]. Genetic algorithm [25], ant colony optimization [26], simulated annealing approach [27], black widow optimization approach [28], whale optimization approach [29,30], firefly algorithm [31,32], interior point method [33], evolutionary programming [34], bat search optimization strategy [35], ant-loin optimization approach [36], and Pareto-optimal front [37] are among the

approaches growingly employed in a variety of complex practical engineering applications. Each of the aforementioned methods for resolving difficult engineering problems has its own advantages and disadvantages, as well as its own efficiency. The optimal solution of these methods is dependent on the input parameters, and it is simple to implement these methods in practice. In contrast to distributed techniques, however, they are computationally expensive and more susceptible to error and attack [38]. The study of the natural world is what inspired all of these techniques.

The adaptive black widow optimization algorithm (ABWOA) was initially presented by [39], and, as a part of the family of artificial intelligence systems [40,41], it achieves the solution of non-convex practical engineering problems regardless of their initial conditions. The structure of the algorithm is simple, and it only requires a limited number of parametric settings.

This study's primary objective is to demonstrate the successful application of a modified ABWOA, known as the adaptive ABWOA method, for solving non-convex IHP model equations. This contrasts with the antecedent literature, which solely takes into account linear restrictions or convex variables [42,43]. Moreover, our approach distinguishes itself through its adaptable nature. The methodology being proposed demonstrates a remarkable ability to dynamically adjust its behavior or parameters during the optimization process, based on the problem's characteristics or the effectiveness of the algorithmic strategy. The algorithms demonstrate a notable ability to adjust and improve their search techniques over time, leading to increased levels of efficiency and effectiveness when faced with complex optimization problems. By avoiding local optimal solutions, the adaptive ABWOA guarantees faster optimization and greater confidence in discovering the global optimal. The inverter depicted in Figure 1 has been optimized using the algorithm provided in this study, and the results have been verified by simulation and experimentation. Nonetheless, the presented method has a vast array of possible applications and can be utilized to solve a number of theoretical and applied challenges. The structure of the paper is as follows. Sections 1 and 2 cover the optimization target inverter introduction and fundamental operation. The problem computing paradigm is explained in Section 3. Section 4 covers results from simulations and experiments, while, in Section 5, the most significant conclusions are provided.

2. Basic Philosophy of Mono-Switch E Class Inverter

As shown in Figure 2, the flipping cycle T_s consists of two separate instances for inverter steady-state performance. For mode I, the transistor is active, and the saturating i_s current increases exponentially throughout the given period T_1 where $U_C = U_d$. In mode II, the state of the transistor changes, and, for the duration of the provided period T_2, it does not conduct. It can be shown from Figure 2 that, during this mode, the capacitor will discharge at a point where it acts as a series resonant circuit where $i_s = 0$, and this state persists until zero current *io*. The combined sum of flipping periods T_1 and T_2 can be denoted by T_s, which is known as the total flipping cycle.

When the transistor is turned on in its efficient operating position, no voltage is applied to it and no current flows through it. Furthermore, it is turned off at zero voltage, so there are no losses when it is not in use. When running at optimal performance, the least amount of energy is wasted and the highest level of productivity is achieved. Additional modes of operation exist, such as below-optimal modes of operation, which are discussed in the literature [44,45].

The following assumptions are made for modeling the inverter depicted in Figure 2:

Assumption 1. *All circuitry elements shown in Figure 2 have ideal characteristics;*

Assumption 2. *The source voltage remains the same throughout the switching period;*

Assumption 3. *The inverter maintains robust performance and uses soft switching.*

The waveforms of current and voltage can be calculated using the following equations:

$$
i_{on}(\phi_s \cdot \tau) = \begin{cases} \chi + [i_{on}(0) - \chi] \cdot \exp\left(-\dfrac{2(\phi_s \cdot \tau)}{\phi_{sm}\sqrt{4\chi^2-1}}\right), \\[2mm] for \quad 0 < \phi_s \cdot \tau \le 2\pi\ell. \\[2mm] \exp\left(-\dfrac{(\phi_s \cdot \tau) - 2\pi\ell}{\phi_{sm}\sqrt{4\chi^2-1}}\right) \\[2mm] \times i_{on}(2\pi\ell) \cdot \cos\left(\dfrac{(\phi_s \cdot \tau) - 2\pi\ell}{\phi_{sm}}\right) + \dfrac{2\chi - i_{on}(2\pi\ell)}{\sqrt{4\chi^2-1}} \\[2mm] \times \sin\left[\left(\dfrac{(\phi_s \cdot \tau) - 2\pi\ell}{\phi_{sm}}\right)\right], \\[2mm] for \quad 2\pi\ell \le (\phi_s \cdot \tau) \le 2\pi. \end{cases} \tag{1}
$$

$$
u_{Cn}(\phi_s \cdot \tau) = \begin{cases} 1, \quad for \quad 0 < \phi_s \cdot \tau \le 2\pi\ell. \\[2mm] \exp\left(-\dfrac{(\phi_s \cdot \tau) - 2\pi\ell}{\phi_{sm}\sqrt{4\chi^2-1}}\right). \\[2mm] \times \left\{\cos\left(-\dfrac{(\phi_s \cdot \tau) - 2\pi\ell}{\phi_{sm}}\right) + \right. \\[2mm] \left. \dfrac{1}{\sqrt{4\chi^2-1}}\right\} \\[2mm] \left[1 - 2\chi^2\left(1 - \exp\left(\dfrac{4\pi\ell}{\phi_s\sqrt{4\chi^2-1}}\right)\right)\right] \\[2mm] \times \sin\left(\dfrac{(\phi_s \cdot \tau) - 2\pi\ell}{\phi_{sm}}\right), \\[2mm] for \quad 2\pi\ell \le (\phi_s \cdot \tau) \le 2\pi. \end{cases} \tag{2}
$$

$$
u_{Tn}(\phi_s \cdot \tau) = 1 - u_{Cn}(\phi_s \cdot \tau), \\ for \quad 0 < \phi_s \cdot \tau \le 2\pi. \tag{3}
$$

$$
\begin{cases} i_{on} = \dfrac{i_o \cdot y_o}{\mu_d}; u_{Cn} = \dfrac{u_c}{\mu_d}; u_{Tn} = \dfrac{u_T}{\mu_d}; \\[2mm] \delta = \dfrac{T_1}{T_s}; \phi_{sn} = \dfrac{\phi_s}{\phi_o}; \phi_s = \dfrac{2\pi}{T_s}; \\[2mm] y_o = \sqrt{\dfrac{L_0}{C}}; \phi_o = \sqrt{\dfrac{1}{L_o C} - \left(\dfrac{R_o}{2L_o}\right)^2}; \\[2mm] \chi = \dfrac{\sqrt{\frac{L_0}{C}}}{R_o}; \end{cases} \tag{4}
$$

Changing the requirements in order to obtain optimal performance (see (5)), by plugging in (1) to (3), we obtain a system of the model represented by (6) and (7):

$$
u_T(2\pi) = 0; \frac{du_T}{dt}(2\pi) = 0 \Rightarrow i_o(2\pi) = 0. \tag{5}
$$

$$
\mathcal{F}_1(\delta, \phi_{sn}) = \left[1 - e\left(-\frac{4\pi \cdot \delta}{\phi_{sn}\sqrt{4\chi^2-1}}\right)\right] \\[2mm] \times \cos\left(\frac{2\pi \cdot (1-\delta)}{\phi_{sn}}\right) + \left[1 + e\left(-\frac{4\pi \cdot \delta}{\phi_{sn}\sqrt{4\chi^2-1}}\right)\right] \\[2mm] \times \frac{\sin\left(\frac{2\pi \cdot (1-\delta)}{\phi_{sn}}\right)}{\sqrt{4\chi^2-1}}. \tag{6}
$$

$$\mathcal{F}_2(\delta, \phi_{sn}) = e\left(-\frac{4\pi \cdot \delta}{\phi_{sn}\sqrt{4\chi^2-1}}\right)\left\{\cos\left(\frac{2\pi \cdot (1-\delta)}{\phi_{sn}}\right)\right.$$
$$+ (1 - 2\chi^2) \cdot \left[1 - e\left(-\frac{4\pi \cdot \delta}{\phi_{sn}\sqrt{4\chi^2-1}}\right)\right]$$
$$\left. \times \frac{\sin\left(\frac{2\pi \cdot (1-\delta)}{\phi_{sn}}\right)}{\sqrt{4\chi^2-1}}\right\} - 1. \tag{7}$$
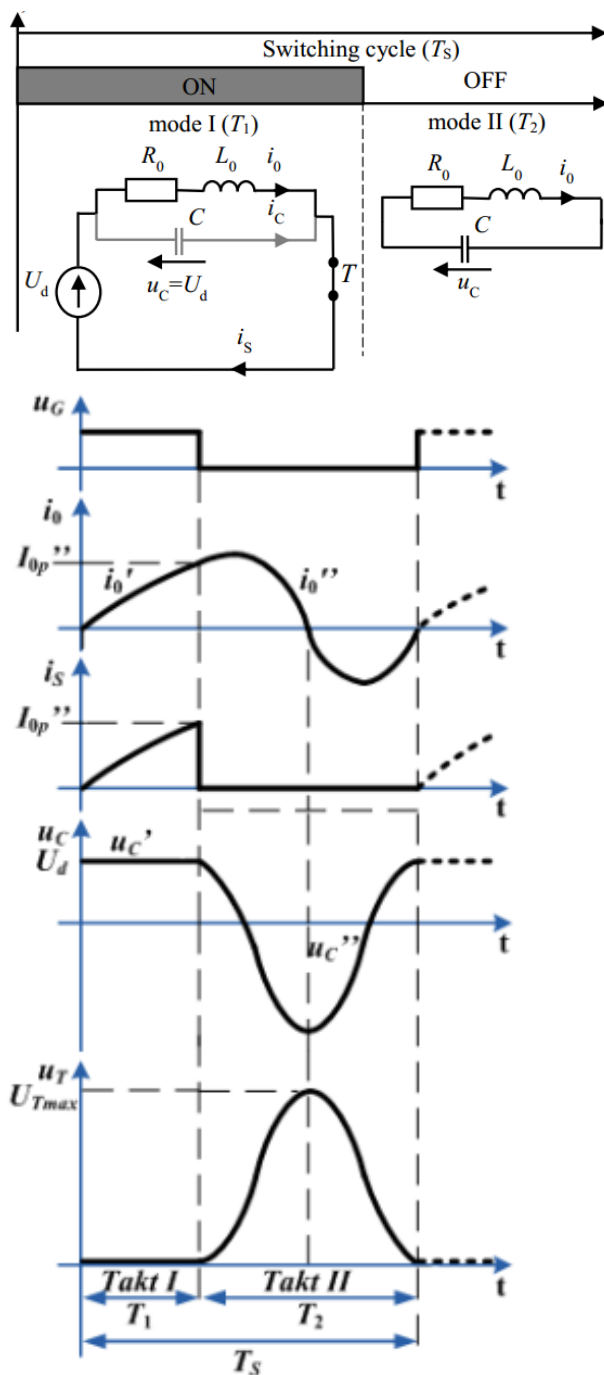

Figure 2. Inverter mode I and mode II comparable designs.

Finding the ideal position of the inverter in which switching losses are reduced is the objective of the optimization. This is accomplished by reducing these two variables (δ and ϕ_{sn}) with the help of the Expression (8):

$$\mathcal{Y}(\delta, \phi_{sn}) = |\mathcal{F}_1(\delta, \phi_{sn})| + |\mathcal{F}_2(\delta, \phi_{sn})| \tag{8}$$

The circuit characteristics of the inverter represented in Figure 1 were obtained as a result of comprehensive measurements conducted under a variety of loads and at a number of frequency ranges. In this study, two scenarios are examined:

1. ***Scenario-I:*** $L_o = 2.1e^{-13}$ MH, $C = 2.4e^{-13}$ MF, $R_o = 8.8e^{-9}$ MΩ, $\chi = 12.8$, and $f_o = 6.067e^{-7}$ THz;
2. ***Scenario-II:*** $L_o = 4.3e^{-13}$ MH, $C = 2.4e^{-13}$ MF, $R_o = 3.5e^{-7}$ MΩ, $\chi = 3.9$, and $f_o = 5e^{-7}$ THz.

The numerical minimization of model (8) was performed in Matlab using the Nelder–Mead approach.

The assumptions of the query have a significant impact on how the problem (8) should be solved. Because we were familiar with the profile of the investigated surface (Figure 3), we were able to make an accurate assumption that, in the end, led us to the correct response.
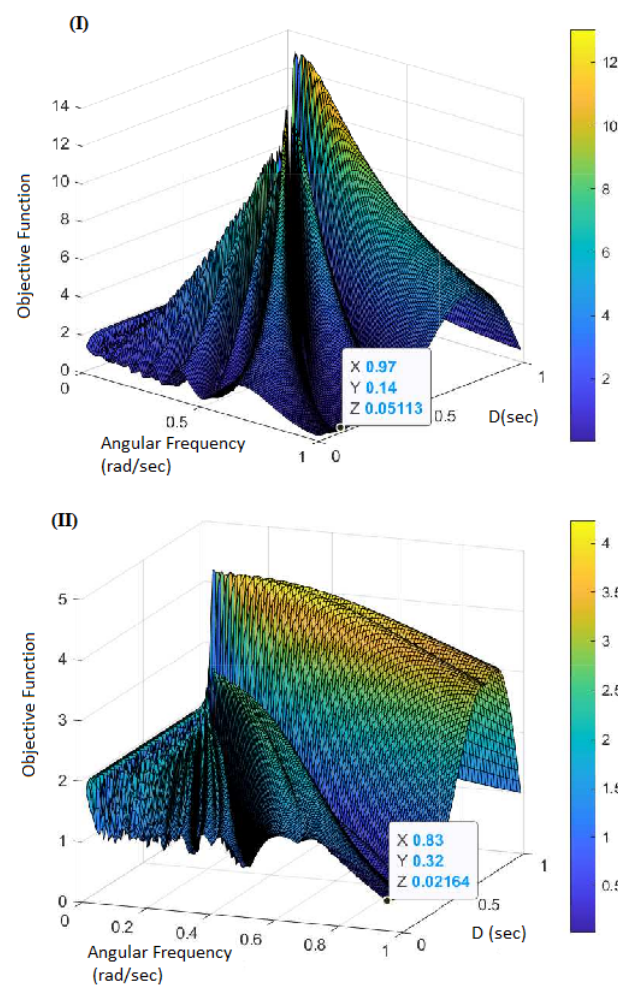

Figure 3. Surfaces of obtaining investigations for scenarios (**I**) and (**II**).

Nevertheless, imaging is required in order to select a starting point that has a good chance of being successful, because the structure of the surface is dependent on the quality parameter χ. The subsequent fireflys were discovered by employing the preceding method (with $\delta = 0.1$ and $\phi_{sn} = 0.99$ as initial values):

1. $(a): \delta = 0.1258$, $\phi_{sn} = 0.98$, $y = 3.385 \times 10^{-5}$, $\phi_s = 3{,}731{,}886$ rad/s, and $f_s = 593.94$ kHz, $t_1 = 0.211$ µs, $t_2 = 1.419$ µs;
2. $(b): \delta = 0.3231$, $\phi_{sn} = 8.3 \times 10^{-1}$, $y = 6.83 \times 10^{-5}$, $\phi_s = 2{,}588{,}401$ rad/s, and $f_s = 2{,}588{,}986{,}505$ rad/s, $t_1 = 0.7841$ µs, $t_2 = 1.6431$ µs.

3. Proposed Adaptive Computing Paradigm

Recently, soft computing frameworks have garnered a lot of interest from researchers all over the world [27] as a result of their versatility and applicability in the process of resolving practical constraint-confined engineering challenges [46–51]. The ABWOA algorithm was inspired by the black widow's cooperative nature [52]. Black widow spiders (BWS) are nocturnal; the females hide throughout the daytime and weave their webs after darkness falls. Widows tend to remain in identical homes for the entirety of their adulthood. If a female spider is ready to interbreed, she sprays pheromones at strategic locations in its web. When an individual joins a web, it weakens the attraction of the site to potential predators.

ABWOA, which was first presented by Hayyolalam [53] and is inspired by the breeding strategy of spiders, has been implemented to tackle a variety of technical and research challenges due to its simplicity and adaptability. Eating is a special step in this process. Through each step, individuals with poor viability are weeded out of the population, hastening consensus; therefore, ABWOA is a great option for optimization systems with many regional minima.

3.1. BWS Biological Lifespan

Tarantulas are crustaceans that inhabit the atmosphere. They have eight legs that terminate in venomous jaws. They constitute the majority of the spider kingdom and are the seventh-most varied group of animals overall. Since 1900, more than 20 categories have been offered, yet there is still controversy among academics as to how numerous species should be classified. The dreaded BWS are members of the Latrodectus spider genus and are feared for the severe toxicity of their fangs. This group is comprised of 30 species and can be found in all parts of the planet [54].

3.1.1. Breeding Mechanism of BWS-Based Optimization

Every "spider" in the BWS framework's beginning swarm represents a potential answer. By mating with one another, the earliest spiders attempt to form a new breed. The female BWS will consume the companion when they are bonding or shortly after. She then carries male gametes in sexual thecae and deposits them in egg vesicles. Spiderlings can hatch from their egg vesicles as soon as 11 nights after being laid. Sibling rivalry occurs during their time together on the postpartum web, which can last up to a week. They are carried away by the wind and vanish.

Logical Steps in ABWOA

Initializing Swarming: To resolve an optimization model, the frequencies of the input parameters must take on a pattern conducive to finding a workable answer. This pattern is classified as a chromosome in genetic algorithm (GA) terminology and as a unit location in particle swarm optimization (PSO) terminology; however, in ABWOA, it is classified as a widow. In ABWOA, every challenge was already equated to a BWS, and the viable answer was viewed as a spider. The challenge parameters' levels are displayed in each BWS. To address the benchmark functions presented in (8), the architecture can be thought of as an aggregate. A widow is an arrangement of size $1 \times n_{var}$ that represents the optimal resolution to an optimization process with n_{var} dimensions. Thus, calculating a widow's resilience using the fitness function is as follows:

$$Fitness = f(widow) \tag{9}$$

Starting generation of arachnid (n_{gen}) is used to build a prospective widow matrix (n_{var}) for the optimization procedure. The next phase is for an arbitrarily picked set of progenitors to engage in sexual reproduction, at which point the female black widow will consume her male counterpart. Thus, the resolution rate and accuracy are both diminished because of the abundance of incorrect choices. As a result, we suggest an innovative idea

for resolving this issue. An alternative method is offered to eliminate the flaws. The heavier the level of pheromones, the nearer the spider is to the optimum solution. To calculate the scent intensity, the program takes into account the mass of every female:

$$\varepsilon_i = \frac{f(x_i) - f_w}{f_b - f_w}. \tag{10}$$

wherein f_w as well as f_b indicate the current generation's weakest and strongest fitness levels.

Offspring Production: Because the couples are autonomous, they begin mating simultaneously to form a new offspring; in the wild, each pair mates in its own web, far behind the rest. In nature, each successful pairing produces around a thousand larvae, but only a fraction of these make it to adulthood. Therefore, in this reproducing mechanism, the widow arrangement must hold arbitrary values, and the progeny are generated by substitution into the following formula:

$$\begin{cases} I_1 = p \times x_1 + (1 - q) \times x_2, \\ I_2 = p \times x_2 + (1 - q) \times x_1. \end{cases} \tag{11}$$

In (11), I_1 and I_2 are children, whereas x_1 and x_2 are parents. The above procedure is carried out $n_{var}/2$ times, with the expectation that no two arbitrary variables will ever be identical. At last, the family unit as a whole (mother and babies) is merged to an arrangement and ranked by fitness, this time taking into account the cannibalism score, with the best candidates being kept for the freshly formed generation. All possible combinations of the following stages are covered here.

Cannibalism: Cannibalism in its three types is represented here. The first is a form of sexual cannibal, where the female black widow consumes her spouse either before or after her act of breeding. Male and female identities in this system were determined by respective fitness scores. The dominant spider lees consume their lesser offspring, which is an example of an offspring cannibal. The proportion of survivors is calculated based on a cannibal score (CS) we establish in this method. The third type of cannibalism is occasionally seen, and it consists of young spiders eating their parents. In order to tell which spider lees are robust and which are feeble, we look at their best fitness.

Mutation: At this point, a sample of the community equal to mutagen has been picked arbitrarily. The various optimal answers shown in Figure 4 involve an arbitrary swap of two items of the arrangement. The rate of mutation is used to determine the mutagen.

There are three possible termination criteria that can be used with dynamic programming: (A) a set number of repetitions; (B) the fitness level of the strongest widow has been stable across several trials; (C) obtaining the targeted degree of precision. The next part of this article focuses on using ABWOA to solve some standard multi-objective optimization problems in (8). The precision level of experimental techniques can be determined by their ability to achieve the given degree of precision.
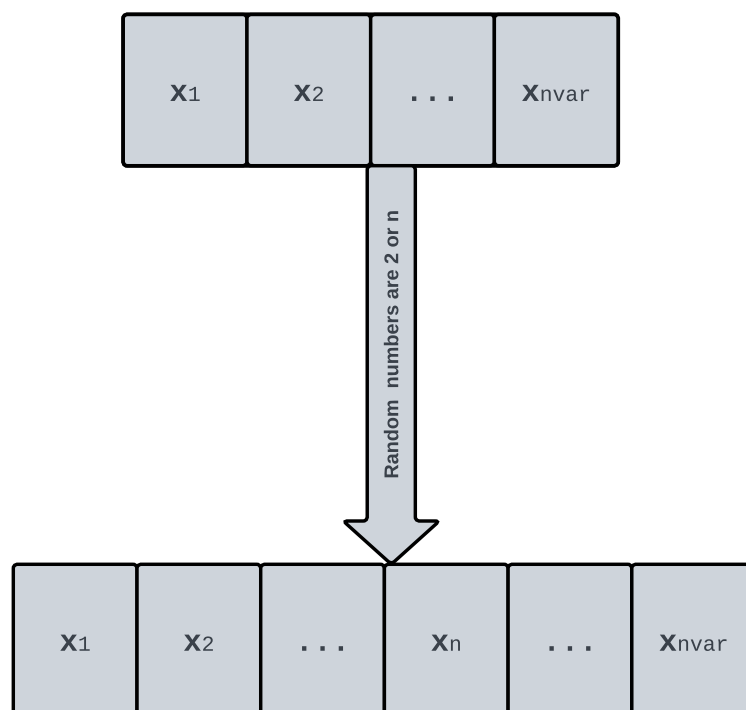
Figure 4. Mutation procedure.

3.1.2. Adjusting the Configuration

Certain attributes in the suggested ABWOA are necessary for optimizing performance, such as mutation score (MS), procreating score (PS), and cannibalism score (CS). By adjusting the settings, the performance of the technique for discovering the optimal solution can be boosted. Improved calibration of additional variables increases both the probability of escaping any localized optimum and the size of the solution space that may be searched. Thus, sufficient qualities permit the exploration and exploitation phases to coexist in controlled concord:

- The proportion of participants who should take part in reproducing is equal to the PS. By regulating the progeny produced, this variable increases diversity and opens up more avenues for inquiry;
- The cannibal function eliminates undesirable members of the colony based on the value of the governing factor, CS. The exploitation stage's effectiveness can be improved by setting the appropriate level for this option;
- PS denotes the percentage of individuals who mutate. Each variable can direct the search individuals' movement from the global to the localized phase, propelling it closer to the ideal alternative.

The ABWOA algorithm exhibits exceptional search proficiency in the detection of global minima in optimization problems. During the exploratory phase, the algorithm facilitates the displacement of spider-like windows across the search space, emulating the hunting behaviors of arachnids. This stage promotes a methodical exploration of various domains, which aids in the recognition of potential global minima. In the exploitation phase, the algorithm proficiently creates complex networks around the most favourable solutions, thus establishing tactical snares to capture potential targets. The utilisation of this specific mechanism enables the algorithm to converge towards global minima by gradually displaying a bias towards solutions that demonstrate more potential. The ABOWA flowchart for the problem in (8) is depicted in Figure 5. In this research, the process was tweaked so that the best population was shifted across all of the dimensions determined by the next-best generation, leading to an enhanced representation of the ABWOA system.
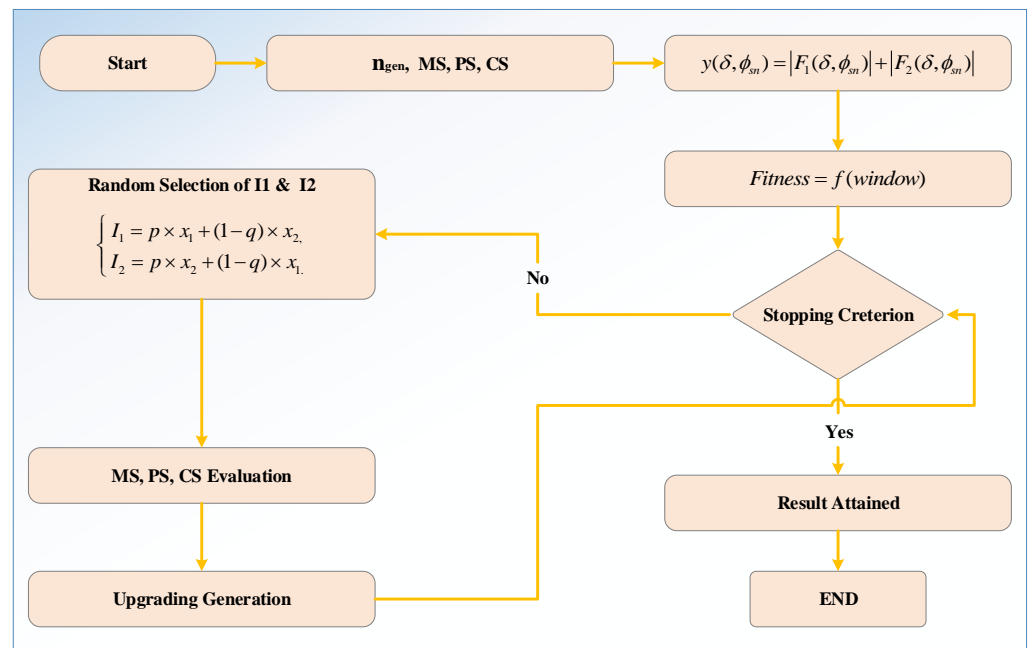
Figure 5. Flowchart of ABWOA.

4. Simulation and Results

In Figure 1, the shifting frequency f_s as well as the propagation time t_1 of the device are required for the effective operation of the inverter. Results were calculated on the basis of the objective function δ and ϕ_{sn} as in (4), by employing an ABWOA paradigm generated by optimizing variable $\mathcal{Y}$ in problem (8) for both scenarios of the inverter's design settings (12):

$$[\delta, \phi_{sn}]^* = \arg\min \mathcal{Y}(\delta, \phi_{sn}). \tag{12}$$

In Equation (12), $[\delta, \phi_m]^*$ indicates the best trade-off values for the objective function under the limitation listed below:

$$0 < \delta < 1, 0 < \phi_{sn} < 1.$$

Using an optimal control technique, we may direct the BW to move in the direction of the decreasing fitness function. The amount of the goal parameter $\mathcal{Y}$ is indicative of the effectiveness of the response to the problem represented by the mutation of the widows x. To keep things simple, we write the BWS coordinates as a pair of numbers, $[\delta, \phi_{sn}]$. The main findings emerged are as follows:

1. *(a)*: $\delta = 0.1256$, $\phi_{sn} = 0.9774$, $y = 1.557 \times 10^{-16}$, $\phi_s = 3{,}721{,}985$ rad/s, and $f_s = 592.373$ kHz, $t_1 = 0.2120$ µs, $t_2 = 1.4761$ µs;
2. *(b)*: $\delta = 0.3678$, $\phi_{sn} = 0.8429$, $y = 3.056 \times 10^{-15}$, $\phi_s = 2{,}622{,}943$ rad/s, and $f_s = 417.454$ kHz, $t_1 = 0.8811$ µs, $t_2 = 1.5144$ µs.

Figure 6 illustrates the optimization of the ABWOA technique that was executed. Following a series of roughly 30 iterations, a result was obtained that bore a striking resemblance to the outcome produced by the fmin optimization algorithm. This outcome was obtained upon the technique's attainment of an approximate number of iterations. The ABWOA methodology was implemented across various experimental paradigms, yielding consistent outcomes. It is imperative to consider that the efficacy of the fmin search instrument was limited to the identification of a resolution solely at the optimal initial point, ascertained by the χ value.
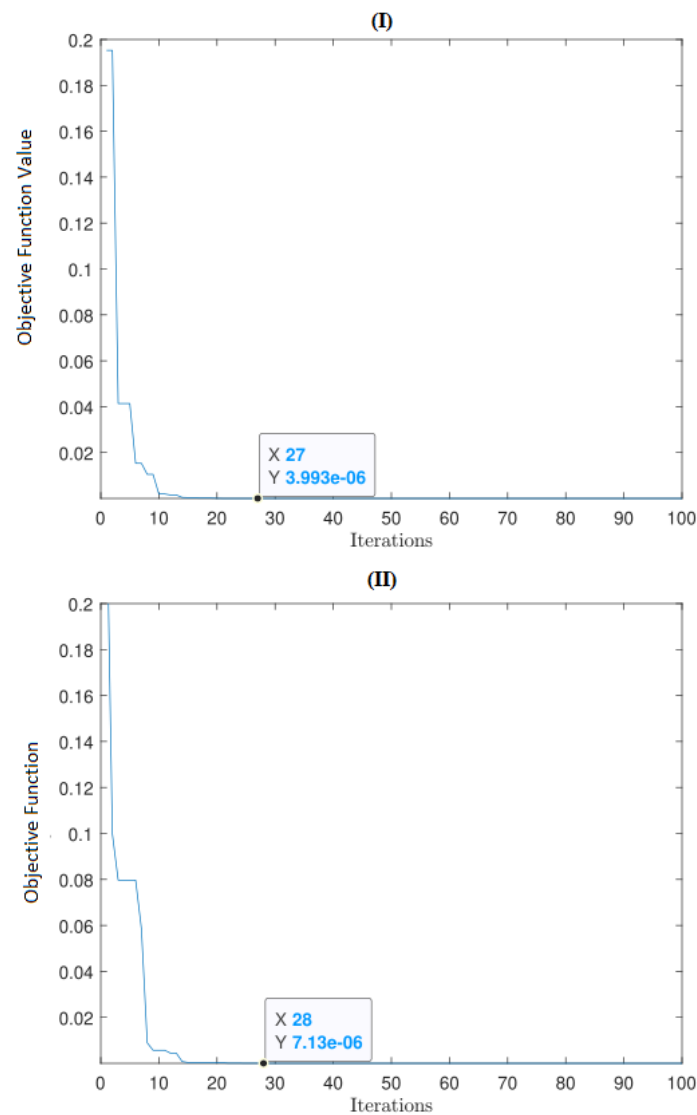
Figure 6. Strategy for optimization using the ABWOA paradigm for scenarios (**I**) and (**II**).

It is of utmost significance to duly acknowledge the temporal duration required for the algorithmic computation of the provided function. The temporal duration necessary for ABWOA to ascertain the resolution was 4.59 s. The aforementioned calculations were executed utilising a computing device that was outfitted with an 11th Generation Intel(R) Core(TM) i7-1165G7 processor, operating at a frequency of 2.80 gigahertz, 16 gigabytes of DDR3 random access memory, a high-density solid-state drive, the 64-bit version of the Windows 10 operating system, and the Matlab 2021a software package. It is of paramount significance to observe that the purported ABWOA not only attained a commendable optimal result, but also fulfilled the pragmatic constraints imposed by the hardware. Furthermore, when juxtaposed with the fmin methodology illustrated in Figure 7, the ABWOA algorithm showcased in Figure 6 evinces a markedly superior optimal value of the objective function expounded in Equation (8) over the identical iteration. One may assess the differentiation between ABWOA and fmin search by juxtaposing the outcomes depicted in Figure 6.
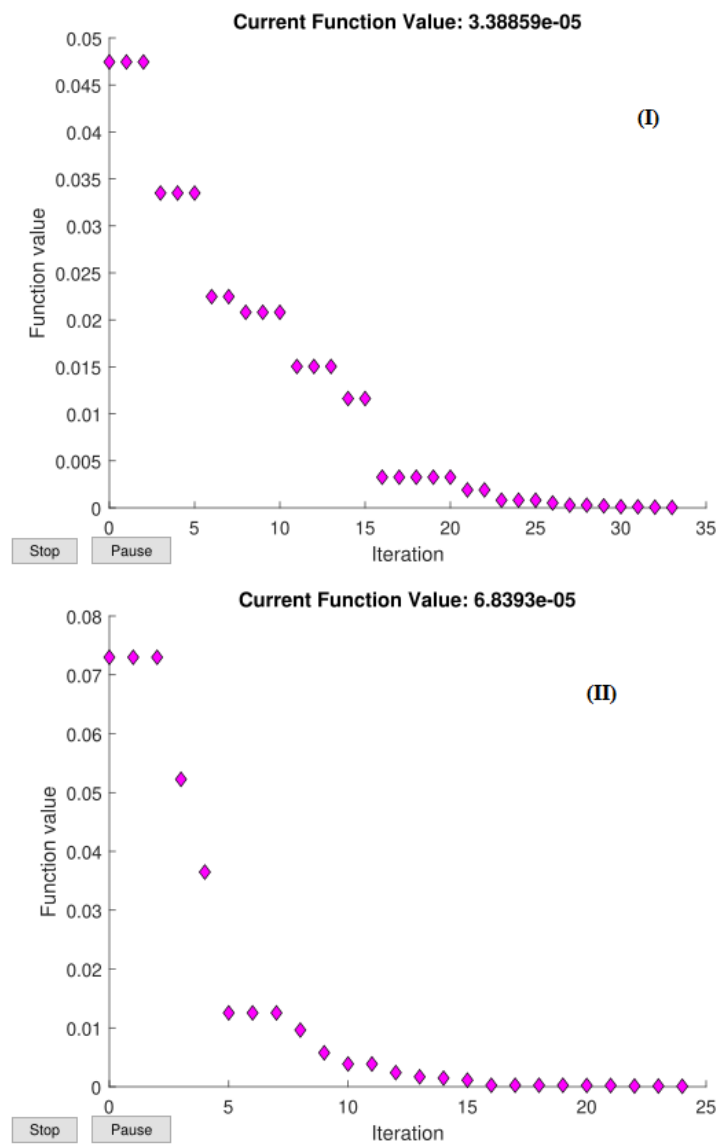
Figure 7. Strategyfor optimization using the *fmin* search for scenarios (**I**) and (**II**).

In addition, the convergence of ABWOA is significantly more precise with a restricted instant of time. Therefore, the results that were obtained reveal that ABWOA is superior to the other approaches in terms of the amount of time it takes to execute, the accuracy it achieves, and the robustness it possesses. In Figure 8, we see the relationship between the quality parameter χ, as well as the normalizing flipping angular frequency ϕ_{sn} and the switching frequency δ. If the parameter χ_{min} is high enough, then the curves can perform at their best. For the proportions of L_o and C chosen, the minimum response is equivalent to 2.606, making the higher resistance $R_{omax} = 4 \times 10^{-3} K$ in scenario 1 and $R_o max = 5 \times 10^{-3} K$ in scenario 2. Tiny tweaks in R_o and L_o have a significant effect on the variables ϕ_{sn} and δ for moderate amounts of χ.
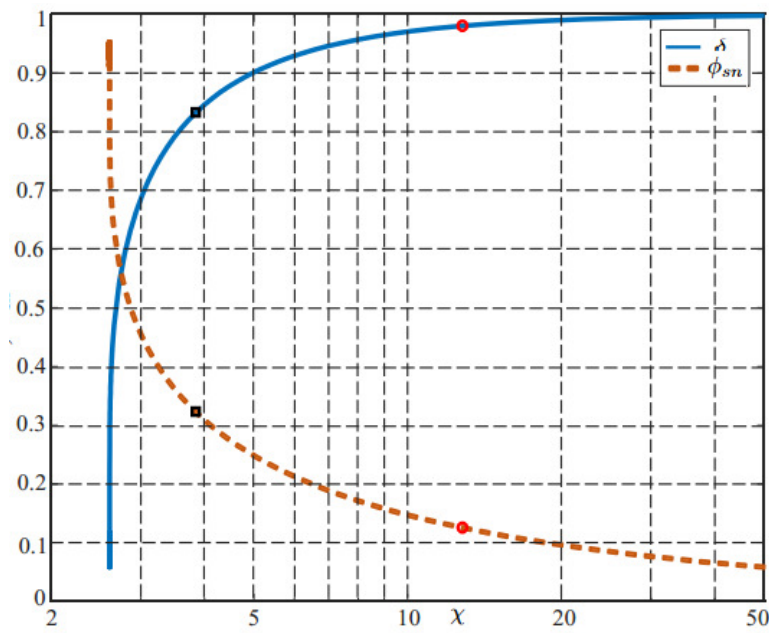
Figure 8. Normalized plot curves.

5. Practical Validation of Results

The principal aim of the researchers was to establish a mathematical framework for the inverter expounded upon in Parts I and II. The utilisation of the firefly algorithm was implemented to calculate the requisite nonlinear coefficients. Based on the ethical principles underlying the physical prototype of the converter, this section presents simulated results that have been corroborated by empirical investigations (refer to Figure 9).
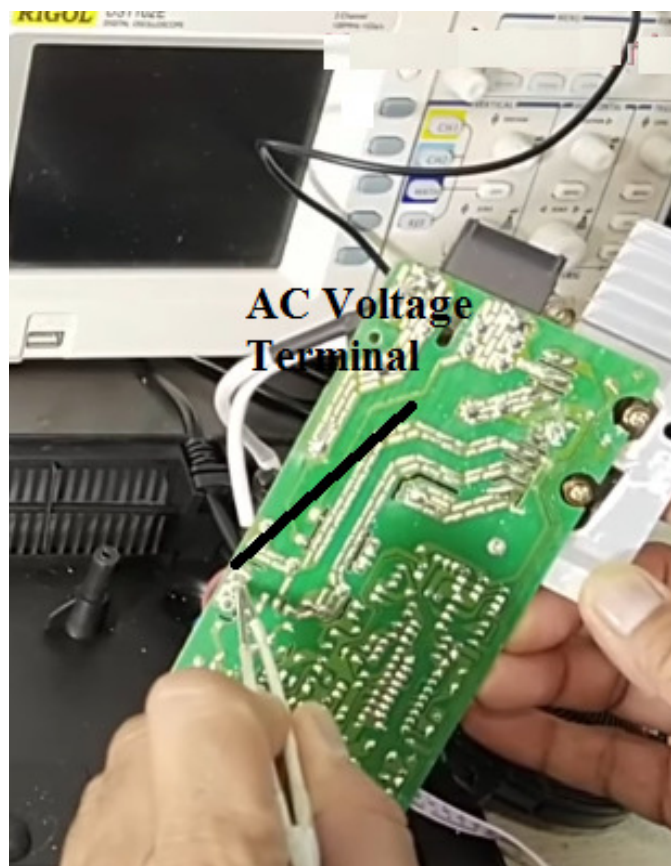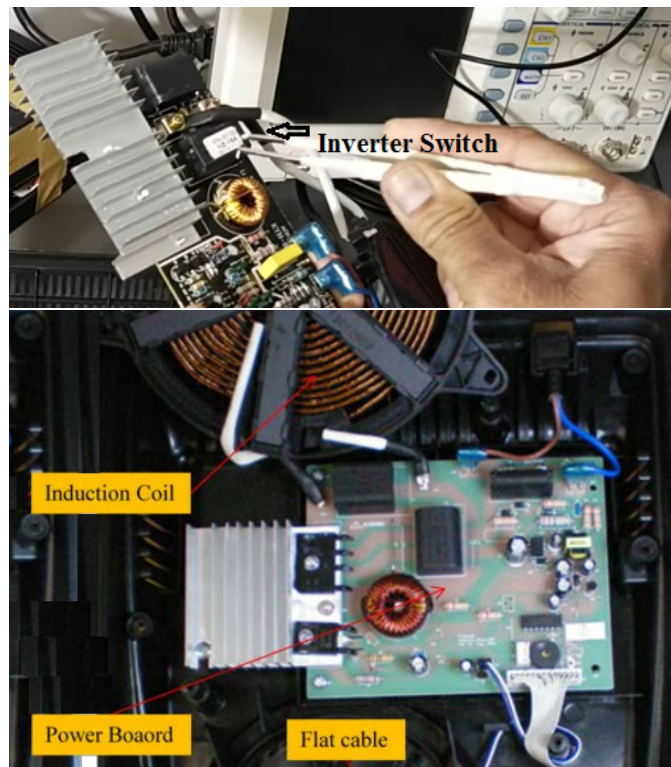

Figure 9. *Cont.*

Figure 9. Prototype design.

Figure 10 displays the most suitable mathematical curves for scenarios 1 and 2, based on a range of qualitative parameters. These curves were approximated using Equations (1) to (3) and the optimal factors identified in Figure 8.
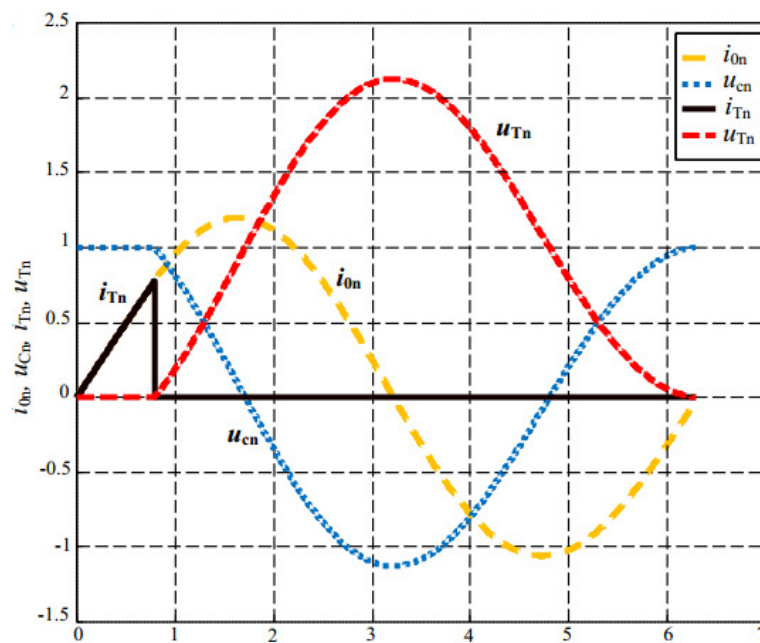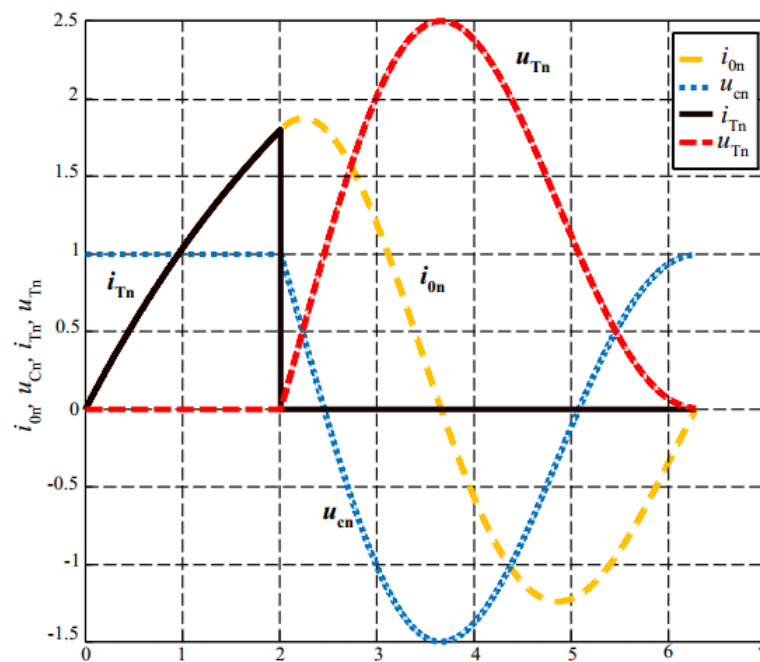

Figure 10. *Cont.*

Figure 10. Estimated optimal operation curves (*i* and *v*) of converter.

The presence of curves serves as a confirmation of the precision of the computed results. To achieve optimal operational efficiency, it is imperative that the potential difference amidst the transistor be reduced to nil upon its reactivation. Moreover, the circuitry that displays a lower quality indicator manifests a conspicuous bias in peak current.

Figure 11 depicts the recorded current and potential curves of an authentic induction cooking converter. The load was comprised of a nonmagnetic shaft measuring 10 mm in thickness, a magnetostrictive filament with a thickness of 4 mm, and an inductance composed of 10 wires. A novel control mechanism has been devised, which possesses the capability to ascertain and sustain the optimal operational posture, regardless of any alterations in the workload's parameters.
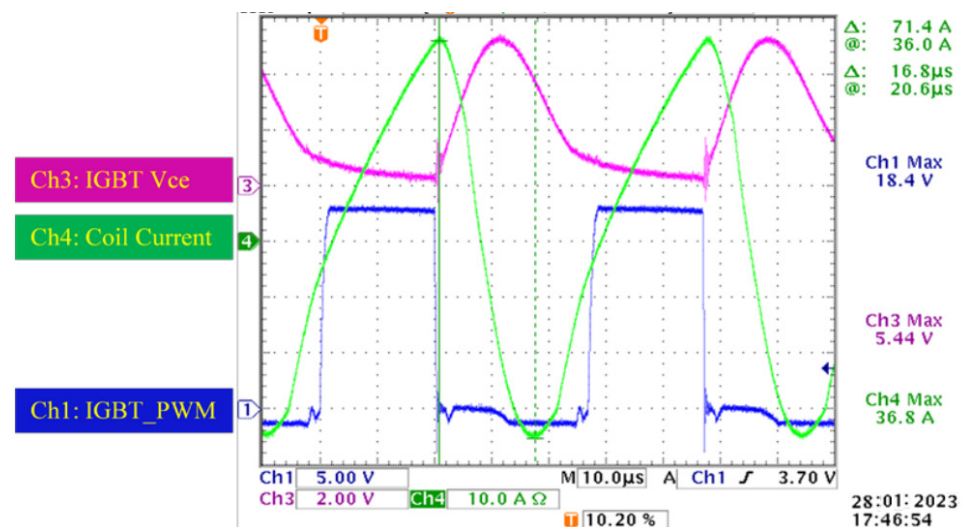

Figure 11. Computed curves in the converter.

Figure 11 shows a curve of the current as well as potential difference that is consistent with the results of the experiment (Figure 10). The transistor begins conducting at very modest potential differences and currents and shuts off at much higher voltages. As a result, there is little damage due to shifting. Residual impedances are not represented, but

their effect on the circuitry is evident. The effects of residual inductances on the potential peak potential difference over the device after it is turned off are particularly interesting.

6. Conclusions

In conclusion, it is vital to showcase the key outcomes of the research in a concise and organized manner. Using bullet points in the conclusion section can effectively highlight the significance of the research outcomes. The main findings of this study are as follows:

The discussed inverter can perform optimally in class E at a substantially higher rate than is usually demonstrated in investigations;

A well-tuned mechanism ensures maximum inverter performance and reduced energy fluctuations at the power-electronic converter;

The adoption of a modern generational converter, such as a SiC semiconductor, mitigates the need for high voltage demand;

The proposed tailored ABWOA scheme method enhances the resolution of real-world issues. The advancements in induction cooking pots are promising and can lead to enhanced culinary experiences, increased ease of use, reduced energy consumption, and heightened ecological viability;

Future research in this field should focus on integrating a greater number of non-linear constraints to attain superior and high-quality optimal solutions.

Overall, these findings have significant implications for the development of energy-efficient and sustainable cooking technologies.

References

1.　Ayub, M.A.; Aziz, S.; Liu, Y.; Peng, J.; Yin, J. Design and Control of Novel Single-Phase Multilevel Voltage Inverter Using MPC Controller. *Sustainability* **2023**, *15*, 860. [CrossRef]
2.　Rasachak, S.; Khan, R.S.U.; Kumar, L.; Zahid, T.; Ghafoor, U.; Selvaraj, J.; Nasrin, R.; Ahmad, M.S. Effect of tin oxide/black paint coating on absorber plate temperature for improved solar still production: A controlled indoor and outdoor investigation. *Int. J. Photoenergy* **2022**, *2022*, 6902783. [CrossRef]
3.　Guillen, P.; Sarnago, H.; Lucia, O.; Burdio, J.M. Series-Resonant Matrix Inverter with Asymmetrical Modulation for Improved Power Factor Correction in Flexible Induction Heating Appliances. *IEEE Trans. Ind. Electron.* **2022**, *70*. [CrossRef]
4.　Plumed, E.; Lope, I.; Acero, J.; Burdío, J.M. Domestic induction heating system with standard primary inductor for reduced-size and high distance cookware. *IEEE Trans. Ind. Appl.* **2022**, *58*, 7562–7571. [CrossRef]
5.　Salvi, B.; Porpandiselvi, S.; Vishwanathan, N. A Three Switch Resonant Inverter for Multiple Load Induction Heating Applications. *IEEE Trans. Power Electron.* **2022**, *37*, 12108–12117. [CrossRef]
6.　Qais, M.; Loo, K.; Liu, J.; Lai, C.M. Least Mean Square Based Fuzzy C-Means Clustering for Load Recognition of Induction Heating. *IEEE Trans. Instrum. Meas.* **2022**. [CrossRef]
7.　Oncu, S.; Unal, K.; Tuncer, U. Laboratory setup for teaching resonant converters and induction heating. *Eng. Sci. Technol. Int. J.* **2022**, *28*, 101012. [CrossRef]
8.　Jang, E.; Kwon, M.J.; Park, S.M.; Ahn, H.M.; Lee, B.K. Analysis and Design of Flexible-Surface Induction-Heating Cooktop with GaN-HEMT-based Multiple Inverter System. *IEEE Trans. Power Electron.* **2022**, *37*, 12865–12876. [CrossRef]
9.　Edrisian, A.; Goudarzi, A.; Ebadian, M. Investigating the effect of high level of wind penetration on voltage stability by quasi-static time-domain simulation (QSTDS). *Int. J. Renew. Energy Res.* **2014**, *4*, 355–362.
10.　Edrisian, A.; Goudarzi, A.; Ebadian, M.; Swanson, A.G.; Mahdiyan, D. Assessing the effective parameters on operation improvement of SCIG based wind farms connected to network. *Int. J. Renew. Energy Res.* **2016**, *6*, 585–592.
11.　Geetha, V.; Pushpavalli, M.; Abirami, P.; Sivagami, P.; Harikrishnan, R. Virtual Plan of the Domestic Enlistment Warming Framework to Reproduce Electromagnetic Boundaries. In *Advancement in Materials, Manufacturing and Energy Engineering*; Springer: Berlin/Heidelberg, Germany, 2022; Volume I, pp. 575–584.

12. Goudarzi, A.; Kazemi, M. DC Optimal Power Flow through the Linear Programming—In Context of Smart Grid. In Proceedings of the 24th Southern African Universities Power Engineering Conference, Vereeniging, South Africa, 26–28 January 2016.

13. Ke, G.; Chen, Q.; Zhang, S.; Xu, X.; Xu, L. A Single-Ended Hybrid Resonant Converter with High Misalignment Tolerance. *IEEE Trans. Power Electron.* **2022**, *37*, 12841–12852. [CrossRef]

14. Wang, S.; Izaki, K.; Hirota, I.; Yamashita, H.; Omori, H.; Nakaoka, M. Induction-heated cooking appliance using new quasi-resonant ZVS-PWM inverter with power factor correction. *IEEE Trans. Ind. Appl.* **1998**, *34*, 705–712. [CrossRef]

15. Nosan, M.; Pavko, L.; Fisgar, M.; Kolar, M.; Genorio, B. Improving Electroactivity of N-Doped Graphene Derivatives with Electrical Induction Heating. *ACS Appl. Energy Mater.* **2022**, *5*, 9571–9580. [CrossRef]

16. Aziz, S.; Hasan, K.; Yaqub, R.; Ahmad, S.; Faiz, M.T. Identifying Unusual Charging Patterns of Electric Vehicles Using Artificial Intelligence. In Proceedings of the 2022 IEEE PES 14th Asia-Pacific Power and Energy Engineering Conference (APPEEC), Melbourne, Australia, 20–23 November 2022; pp. 1–6.

17. Yin, Y.; Zhang, N.; Zhang, J.; Li, Z.; Jia, Z. Thermal optimization of single crystal fiber manufacturing based on heat loss compensation. *Appl. Therm. Eng.* **2022**, *201*, 117741. [CrossRef]

18. Zhang, J.; Zhao, J.; Mao, L.; Zhao, J.; Jiang, Z.; Qu, K. ZVS Operation of Class-E Inverter Based on Secondary Side Zero Compensation Switching at Variable Coupling Coefficient in WPT. *IEEE Trans. Ind. Appl.* **2021**, *58*, 1022–1031. [CrossRef]

19. Karafil, A.; Ozbay, H.; Oncu, S. Comparison of regular and irregular 32 pulse density modulation patterns for induction heating. *IET Power Electron.* **2021**, *14*, 78–89. [CrossRef]

20. Lundström, F.; Frogner, K.; Andersson, M. Numerical modelling of CFRP induction heating using temperature-dependent material properties. *Compos. Part Eng.* **2021**, *220*, 108982. [CrossRef]

21. Villa, J.; Navarro, D.; Dominguez, A.; Artigas, J.I.; Barragan, L.A. Vessel Recognition in Induction Heating Appliances—A Deep-Learning Approach. *IEEE Access* **2021**, *9*, 16053–16061. [CrossRef]

22. Gillani, F.; Zahid, T.; Bibi, S.; Khan, R.S.U.; Bhutta, M.R.; Ghafoor, U. Parametric Optimization for Quality of Electric Discharge Machined Profile by Using Multi-Shape Electrode. *Materials* **2022**, *15*, 2205. [CrossRef]

23. Maier, H.R.; Razavi, S.; Kapelan, Z.; Matott, L.S.; Kasprzyk, J.; Tolson, B.A. Introductory overview: Optimization using evolutionary algorithms and other metaheuristics. *Environ. Model. Softw.* **2019**, *114*, 195–213. [CrossRef]

24. Aziz, S.; Irshad, M.; Haider, S.A.; Wu, J.; Deng, D.N.; Ahmad, S. Protection of a smart grid with the detection of cyber-malware attacks using efficient and novel machine learning models. *Front. Energy Res.* **2022**, *10*, 1102. [CrossRef]

25. Ahmed, I.; Alvi, U.E.H.; Basit, A.; Khursheed, T.; Alvi, A.; Hong, K.S.; Rehan, M. A novel hybrid soft computing optimization framework for dynamic economic dispatch problem of complex non-convex contiguous constrained machines. *PLoS ONE* **2022**, *17*, e0261709. [CrossRef]

26. Li, M.; Wang, G.G.; Yu, H. Sorting-based discrete artificial bee colony algorithm for solving fuzzy hybrid flow shop green scheduling problem. *Mathematics* **2021**, *9*, 2250. [CrossRef]

27. Ahmed, I.; Rao, A.R.; Shah, A.; Alamzeb, E.; Khan, J.A. Performance of various metaheuristic techniques for economic dispatch problem with valve point loading effects and multiple fueling options. *Adv. Electr. Eng.* **2014**, *2014*, 765053. [CrossRef]

28. Ahmed, I.; Rehan, M.; Basit, A.; Hong, K.S. Greenhouse gases emission reduction for electric power generation sector by efficient dispatching of thermal plants integrated with renewable systems. *Sci. Rep.* **2022**, *12*, 12380. [CrossRef]

29. Ahmed, I.; Basit, A.; Rehan, M.; Hong, K.S. Multi-objective whale optimization approach for cost and emissions scheduling of thermal plants in energy hubs. *Energy Rep.* **2022**, *8*, 9158–9174. [CrossRef]

30. Ahmed, I.; Rehan, M.; Basit, A.; Malik, S.H.; Hong, K.S. Multi-area economic emission dispatch for large-scale multi-fueled power plants contemplating inter-connected grid tie-lines power flow limitations. *Energy* **2022**, *261*, 125178. [CrossRef]

31. Zhang, R.; Li, G.; Bu, S.; Aziz, S.; Qureshi, R. Data-driven cooperative trading framework for a risk-constrained wind integrated power system considering market uncertainties. *Int. J. Electr. Power Energy Syst.* **2023**, *144*, 108566. [CrossRef]

32. Li, J.; An, Q.; Lei, H.; Deng, Q.; Wang, G.G. Survey of lévy flight-based metaheuristics for optimization. *Mathematics* **2022**, *10*, 2785. [CrossRef]

33. Darvay, Z.; Illés, T.; Rigó, P.R. Predictor-corrector interior-point algorithm for P*(κ)-linear complementarity problems based on a new type of algebraic equivalent transformation technique. *Eur. J. Oper. Res.* **2022**, *298*, 25–35. [CrossRef]

34. Qi, R.; Li, J.Q.; Wang, J.; Jin, H.; Han, Y.Y. QMOEA: A Q-learning-based multiobjective evolutionary algorithm for solving time-dependent green vehicle routing problems with time windows. *Inf. Sci.* **2022**, *608*, 178–201. [CrossRef]

35. Essa, K.S.; Diab, Z.E. Magnetic data interpretation for 2D dikes by the metaheuristic bat algorithm: sustainable development cases. *Sci. Rep.* **2022**, *12*, 14206. [CrossRef]

36. Li, Q.; Li, D.; Zhao, K.; Wang, L.; Wang, K. State of health estimation of lithium-ion battery based on improved ant lion optimization and support vector regression. *J. Energy Storage* **2022**, *50*, 104215. [CrossRef]

37. Wang, Y.; Li, K.; Wang, G.G. Combining key-points-based transfer learning and hybrid prediction strategies for dynamic multi-objective optimization. *Mathematics* **2022**, *10*, 2117. [CrossRef]

38. Bogonikolos, N.; Metai, E.; Tsiomos, K. Centralized and Decentralized Optimization Approaches for Energy Management within the VPP. In *Virtual Power Plant Solution for Future Smart Energy Communities*; CRC Press: Boca Raton, FL, USA, 2022; pp. 145–154.

39. Askarzadeh, A. A novel metaheuristic method for solving constrained engineering optimization problems: Crow search algorithm. *Comput. Struct.* **2016**, *169*, 1–12. [CrossRef]

40. Zhang, R.; Aziz, S.; Farooq, M.U.; Hasan, K.N.; Mohammed, N.; Ahmad, S.; Ibadah, N. A wind energy supplier bidding strategy using combined ega-inspired hpsoifa optimizer and deep learning predictor. *Energies* **2021**, *14*, 3059. [CrossRef]

41. Meng, A.; Wang, H.; Aziz, S.; Peng, J.; Jiang, H. Kalman filtering based interval state estimation for attack detection. *Energy Procedia* **2019**, *158*, 6589–6594. [CrossRef]

42. Lucía, O.; Burdío, J.; Millán, I.; Acero, J.; Llorente, S. Efficiency optimization of half-bridge series resonant inverter with asymmetrical duty cycle control for domestic induction heating. In Proceedings of the 2009 13th European Conference on Power Electronics and Applications, Barcelona, Spain, 8–10 September 2009; pp. 1–6.

43. Souley, M.; Egalon, J.; Caux, S.; Pateau, O.; Lefèvre, Y.; Maussion, P. Optimization of the settings of multiphase induction heating system. *IEEE Trans. Ind. Appl.* **2013**, *49*, 2444–2450. [CrossRef]

44. Omori, H.; Yamashita, H.; Nakaoka, M.; Maruhashi, T. A novel type induction-heating single-ended resonant inverter using new bipolar Darlington-Transistor. In Proceedings of the 1985 IEEE Power Electronics Specialists Conference, Toulouse, France, 24–28 June 1985; pp. 590–599.

45. Zhou, Z.; Anwar, G.A.; Dong, Y. Performance-based bi-objective retrofit optimization of building portfolios considering uncertainties and environmental impacts. *Buildings* **2022**, *12*, 85. [CrossRef]

46. Meraihi, Y.; Gabis, A.B.; Ramdane-Cherif, A.; Acheli, D. A comprehensive survey of Crow Search Algorithm and its applications. *Artif. Intell. Rev.* **2021**, *54*, 2669–2716. [CrossRef]

47. Anwar, G.A.; Hussain, M.; Akber, M.Z.; Khan, M.A.; Khan, A.A. Sustainability-Oriented Optimization and Decision Making of Community Buildings under Seismic Hazard. *Sustainability* **2023**, *15*, 4385. [CrossRef]

48. Ahmed, I.; Hasan, S.R.; Ashfaq, B.; Raza, M.; Mukhtar, S. Adaptive Swarm Intelligence-Based Optimization Approach for Smart Grids Power Dispatch. In Proceedings of the 2022 International Conference on Emerging Technologies in Electronics, Computing and Communication (ICETECC), Jamshoro, Pakistan, 7–9 December 2022; pp. 1–6. [CrossRef]

49. Mustafa, F.E.; Ahmed, I.; Basit, A.; Malik, S.H.; Mahmood, A.; Ali, P.R. A review on effective alarm management systems for industrial process control: Barriers and opportunities. *Int. J. Crit. Infrastruct. Prot.* **2023**, *41*, 1043. [CrossRef]

50. Ahmed, I.; Rehan, M.; Basit, A.; Tufail, M.; Hong, K.S. A Dynamic Optimal Scheduling Strategy for Multi-Charging Scenarios of Plug-in-Electric Vehicles over a Smart Grid. *IEEE Access* **2023**, *11*, 28992–29008. [CrossRef]

51. Ahmed, I.; Rehan, M.; Hong, K.S.; Basit, A. A Consensus-based Approach for Economic Dispatch considering Multiple Fueling Strategy of Electricity Production Sector over a Smart Grid. In Proceedings of the 2022 13th Asian Control Conference (ASCC), Jeju, Republic of Korea, 4–7 May 2022. [CrossRef]

52. Schraft, H.A.; Bilbrey, C.; Olenski, M.; DiRienzo, N.; Montiglio, P.O.; Dornhaus, A. Injected serotonin decreases foraging aggression in black widow spiders (Latrodectus hesperus), but dopamine has no effect. *Behav. Process.* **2023**, *204*, 104802. [CrossRef] [PubMed]

53. Hayyolalam, V.; Kazem, A.A.P. Black widow optimization algorithm: A novel meta-heuristic approach for solving engineering optimization problems. *Eng. Appl. Artif. Intell.* **2020**, *87*, 103249. [CrossRef]

54. McCowan, C.; Garb, J.E. Recruitment and diversification of an ecdysozoan family of neuropeptide hormones for black widow spider venom expression. *Gene* **2014**, *536*, 366–375. [CrossRef]